# Plasmonic micropillars for precision cell force measurement across a large field-of-view

Fan Xiao,[1] Ximiao Wen,[1] Xing Haw Marvin Tan,[2] and Pei-Yu Chiou[1,2]

[1]*Department of Mechanical and Aerospace Engineering, University of California at Los Angeles (UCLA), Los Angeles, California 90095, USA*
[2]*Department of Bioengineering, University of California at Los Angeles (UCLA), Los Angeles, California 90095, USA*

A plasmonic micropillar platform with self-organized gold nanospheres is reported for the precision cell traction force measurement across a large field-of-view (FOV). Gold nanospheres were implanted into the tips of polymer micropillars by annealing gold microdisks with nanosecond laser pulses. Each gold nanosphere is physically anchored in the center of a pillar tip and serves as a strong, point-source-like light scattering center for each micropillar. This allows a micropillar to be clearly observed and precisely tracked even under a low magnification objective lens for the concurrent and precision measurement across a large FOV. A spatial resolution of 30 nm for the pillar deflection measurement has been accomplished on this platform with a 20× objective lens. *Published by AIP Publishing.* https://doi.org/10.1063/1.5005525

Mechanical interactions between cells and their extra-cellular matrix environment (ECM) are critical for cellular and biological tissue functions. Versatile tools have been developed for measuring the mechanical properties of cells and their interactions with the extra-cellular matrix. Atomic force microscopy and cantilever beam approaches can provide high sensitivity and high spatial resolution measurements but have low throughputs.[1] Micro-patterned elastomer substrates with embedded markers are easy to fabricate.[2] By detecting the positions of embedded beads, stress and strain information on cells can be extracted. However, it requires complex computational algorithms to accurately extract cell traction forces since the displacement of neighboring markers is coupled. Moreover, different algorithms yielding different values of cell traction forces have been reported, leading to numerical inconsistencies.[3] Elastomer micropillar approaches eliminate this coupling issue by using a discrete pillar array, in which the deflections of neighboring pillars are decoupled.[4] Cell traction forces can be extracted through a simple classical elasticity model. By growing cells on top of densely arrayed micropillars, dynamic traction forces can be measured to understand the processes of mechanical regulations of cell functions,[4] such as cell differentiation,[5] cell migration,[6–8] wound healing,[9] and immunological functions.[10]

In previous micropillar works, the tips of elastomer micropillars are usually labeled with fluorescent markers to facilitate pillar tracking.[5] The center of each pillar can be found by mathematically fitting the fluorescence profile of a pillar tip with a two-dimensional Gaussian function. Precision pillar tracking at a spatial resolution of 30 nm can be achieved with a high numerical aperture (N.A.) objective lens.[11] However, the need of a high magnification and high N.A. lens limits its FOV for concurrent and precision measurements. Furthermore, the fluorescent markers coated on pillars might be chemically degraded or optically damaged over time[12–14]

Here, a plasmonic micropillar platform is reported for concurrent and precision traction force measurements across a large FOV (Fig. 1). There are several unique features of this plasmonic micropillar platform. First, each micropillar has a single gold nanosphere embedded in its tip to serve as a strong light scattering center,[15–20] which is an optical property of plasmonic nanoparticles.[21,22] This allows the tip to be clearly observed even under a low magnification objective lens that typically has low N.A. and low light collection efficiency. Second, these gold nanospheres are physically locked inside the pillar during the laser annealing process. They are mechanically robust and chemically stable. Third, the submicron-sized gold nanosphere is a point-source-like light source. It produces a smooth and symmetric Gaussian intensity profile in the imaging plane under low magnification optics. All optical signals detected on the image plane originate from that single gold nanosphere whose position can be precisely determined using the commonly used Gaussian curve fitting method. This is the key feature that allows this approach to realize precision tracking of the pillar location even under low magnification optics. In previous pillar works that rely on coating of fluorescent molecules or other markers to track their location, the accuracy of curve fitting is impacted by the distribution of fluorescent molecules on a pillar tip that is typically micrometers in size. When imaged under a low magnification optics system, the intensity profile of a single pillar, which is a result of the superposition of all point sources on a pillar, is not symmetric when the coating is not uniform and not circular in shape.[23,24]

A simple Gaussian fitting cannot accurately reflect the true location of a pillar. This is why a high magnification and high
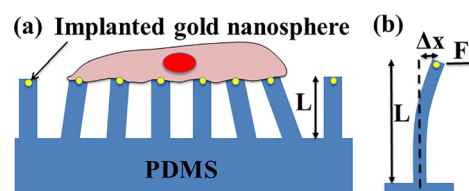


FIG. 1. Schematics of a plasmonic micropillar platform for the cell force measurement. Each polymer micropillar tip is embedded with a single gold nanosphere that serves as a strong and point-source-like light source for precision position tracking.
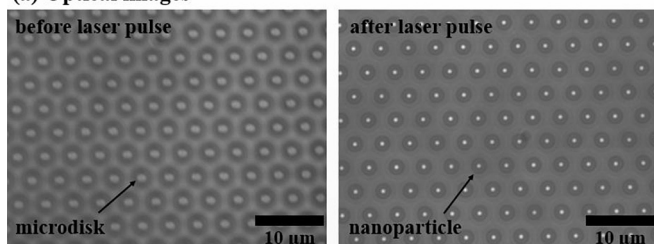
high N.A. objective lens is required to minimize the impacts of coating uniformity on a pillar and between pillars in order to achieve high resolution tracking.[4,7,11,25–27]

The fabrication of a plasmonic micropillar platform starts from a hard silicon mold (see supplementary material, Fig. S1). An uncured Polydimethylsiloxane (PDMS) precursor was poured onto the silicon mold, cured, and then peeled off to create a soft PDMS mold. A composite layer, 20 nm $SiO_2$/1 nm Ti/40 nm Au, was deposited onto this PDMS mold by electron beam evaporation. An adhesive kapton tape was used to remove the composite layer on the surface and leave only the composite layer at the bottom of PDMS wells. Uncured PDMS was then poured onto the PDMS mold and cured.
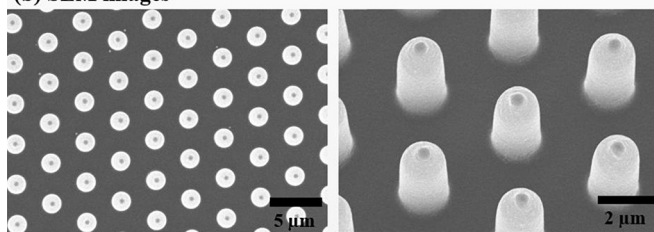
The structure was then laser annealed by scanning nanosecond laser pulses across the chip (Q-switched, Nd:YAG, Minilite I, Continuum Inc., pulse duration 6nsec, wavelength 532 nm, pulse energy 1 mJ, and fluence 400 mJ/cm$^2$). This annealing step melts and transforms the gold microdisks into nanospheres. After laser annealing, the PDMS plasmonic micropillars were peeled off from the mold. Of note here is that, due to the non-uniform Gaussian-shaped intensity profile of the laser beam, gold nanospheres do not form well in regions near the edge of a light beam due to insufficient thermal energy absorbed from light.

The optical and SEM images of the fabricated micropillars are shown in Figs. 2(a) and 2(b). They confirm that there is only one gold nanosphere embedded in each micropillar. The

focused ion beam (FIB, Nova 600) image shown in Fig. 2(c) shows one of the embedded gold nanospheres physically anchored inside a micropillar. It has an oblate spheroid shape with a long axis of 473 nm and a short axis of 268 nm and is circularly symmetric from the top view. Due to the non-uniformity of the laser beam, the gold nanospheres have slightly different dimensions. Near the edge of a laser beam during manufacturing, gold disks do not transform into a single-particle form and cannot be transferred into PDMS pillars. This issue can be solved by using a laser with higher pulse energy that can provide uniform intensity over a larger area.

A dark-field image of a plasmonic micropillar platform taken with a 20×, N.A. 0.5 objective lens and a halogen lamp is shown in Figs. 3(a) and 3(b). The size of the nanosphere is smaller than the optical diffraction limit of this lens and is treated as a single point light source. The intensity profile of a point source in an optical system can be described by the Airy point spread function (PSF). However, its calculation is tedious, and in many practical applications, it is approximated by a 2D Gaussian function. A standard least-squares fitting method is used in the current work for tracking gold nanospheres.[28,29] Figures 3(c) and 3(d) show an example of sub-pixel resolution tracking of a gold nanosphere by utilizing a 2D Gaussian function to fit the digitalized intensity profile.

The signal-to-noise ratio between scattering signals from a gold nanosphere and its surrounding structure is large. Figure 4(a) shows the reference dark field image of pillars without cells. Figure 4(b) shows a dark field image of pillars with cells growing on top. However, due to cells' weak scattering signals compared to gold nanospheres, they are hardly seen under dark-field imaging. To identify cells' locations, the Wheat Germ Agglutinin Alexa Fluor® 594 (WGA 594, Life Technologies) dye was used to stain them for fluorescence imaging [Fig. 4(c)], and a stacked image (dark field + fluorescence) is shown in Fig. 4(d). The signal-to-noise ratio between gold nanospheres and the surrounding cells
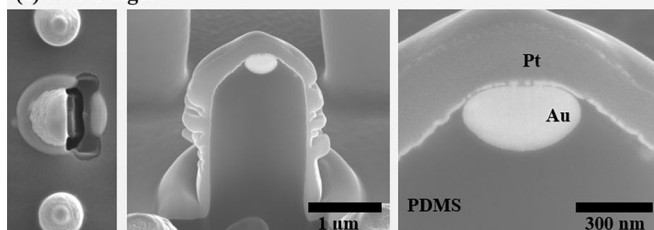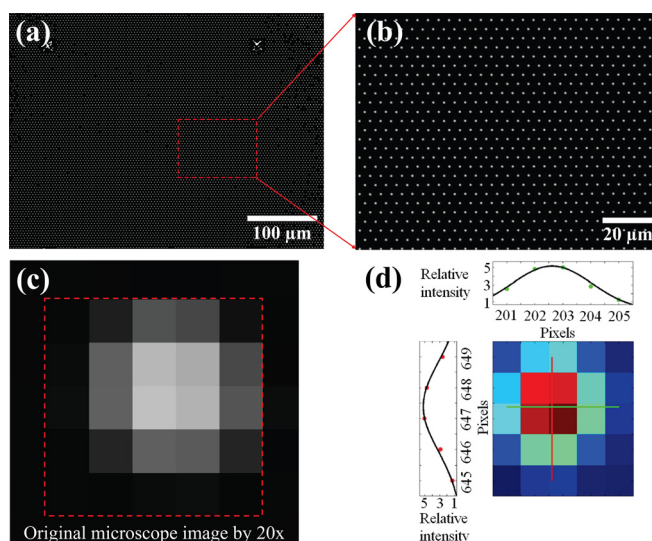


FIG. 2. (a) Microscopy optical images which show that gold microdisks transformed into gold nanospheres after pulse laser annealing. (b) Scanning electron microscopy (SEM) images show micropillars with transferred gold nanospheres. (c) Focused ion beam (FIB) images show that these transferred gold nanospheres are physically anchored inside the pillar and have an oblate spheroid shape with a long axis of 473 nm and a short axis of 268 nm. Platinum (Pt) coating shown in the images is for FIB imaging and not a part of the original pillar structure.



FIG. 3. Sub-pixel resolution position measurement. (a) and (b) Dark-field images of plasmonic micropillars taken by a 20× objective lens (NA 0.5). (c) A zoom-in image of a single gold nanoparticle. Each square pixel represents a dimension of 322.5 nm × 322.5 nm in the dark-field image. (d) The center location of this gold nanoparticle can be accurately measured at a sub-pixel resolution by using the 2D Gaussian fitting method.

**(a) Pillar without cells**

**(b) Pillar with cells**

**(c) Fluorescent image**

**(d) Stacked image**

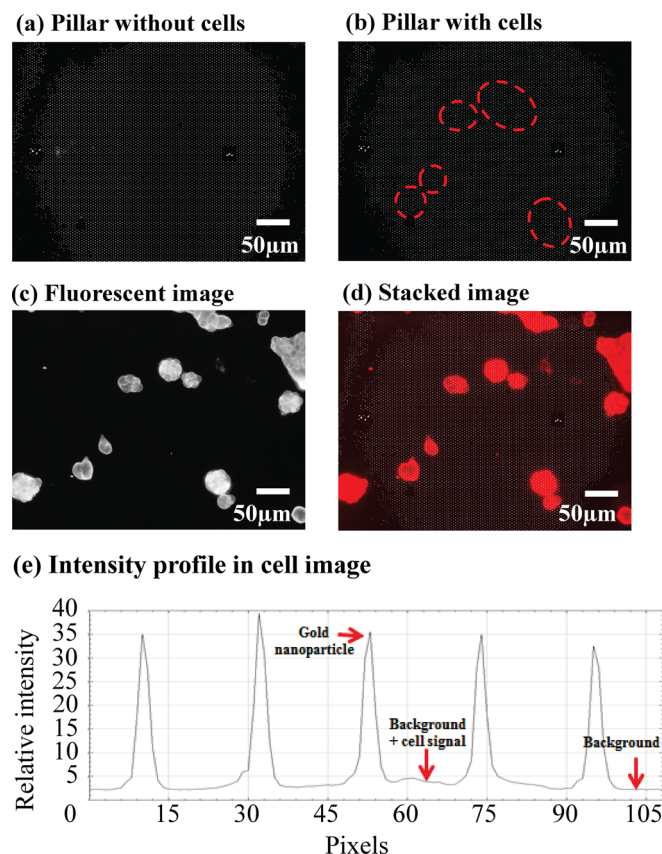**(e) Intensity profile in cell image**

FIG. 4. (a) A reference dark-field image with culture medium but no cell on the platform. (b) A dark-field image with cells loaded on the platform. Pillar bending is clearly observed in the region with cells (red dashed circles), but cells are hardly seen due to their weak scattering signals. (c) A fluorescence image shows cells on the platform. These cells were stained by the red WGA594 dye. (d) A stacked image of (b) and (c). (e) A gray scale intensity plot compares the relative scattering signal strengths from gold nanospheres and surrounding structures. A signal-to-noise ratio above 7 is achieved.

and pillars is above 7 as shown in the intensity profile in Fig. 4(e). The signal-to-noise ratio was calculated by taking the maximum intensity of the gold nanosphere and dividing it by the intensity of the background. The intensity of the gold nanosphere is bright and the signal-to-noise ratio is high, even when the cell's intensity is included in the background intensity.

Cell traction force on a pillar can be calculated by multiplying the pillar deflection by its spring constant. For a long cylindrical-shaped micropillar, the force can be calculated by the following formula:

$$F = \frac{4}{3} \pi E \frac{r^4}{L^3} \Delta x, \tag{1}$$

where F is the traction force, E is the Young's modulus, r is the radius, L is the height of the pillar, and $\Delta x$ is the pillar deflection. For example, if a PDMS micropillar has a diameter of $2\,\mu m$, a height of $10\,\mu m$, and a Young's modulus of $1\,MPa$, the $30\,nm$ spatial resolution gives a random error of $0.36\,nN$ for the cell traction force. For the needs of different applications, the diameter, the height, and the Young's modulus of PDMS may be tuned.

An example of a traction force map measured on a plasmonic micropillar platform by a $20\times$ objective lens is shown in Fig. 5(a). Zoom-in images of the selected regions in Fig. 5(a) are shown in Figs. 5(b)–5(d). Madin-Darby canine kidney (MDCK, Sigma-Aldrich) epithelial cells were
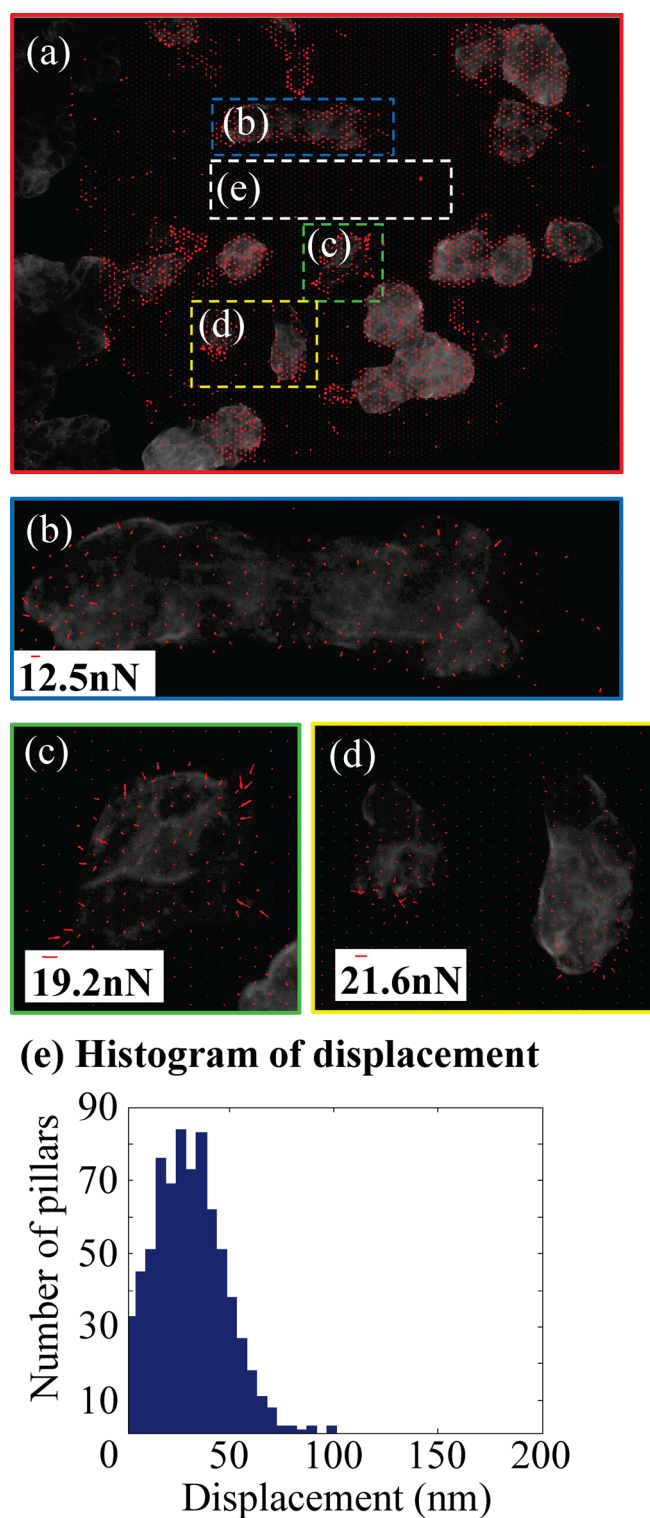
**(e) Histogram of displacement**

FIG. 5. (a) A stacked image (dark field + fluorescence + force map) shows the magnitude and the direction of forces (length and direction red arrow) on a plasmonic micropillar platform. (b)–(d) Zoom-in images of selected regions in (a). (e) Histogram plot of displacements measured in the region "e" where there is no cell. The mean value of these displacements is ~30 nm, which is the tracking resolution of the plasmonic micropillar. The micropillar has a diameter of $1.7\,\mu m$, a height of $5.8\,\mu m$, and a Young's modulus of $2.0\,MPa$.

cultured in the Dulbecco's Modified Eagle Medium (DMEM, Life Technologies) supplemented with 10% fetal bovine serum and 1% penicillin and streptomycin. Non-fluorescent fibronectin (Sigma-Aldrich) was contact-printed on pillar tips to help cell seeding. Other parts of the device

were coated with Pluronic F127 to avoid the undesired attachment of cells. The FOV is $448\,\mu m \times 333\,\mu m$. The micropillar has a diameter of $1.7\,\mu m$, a height of $5.8\,\mu m$, and a Young's modulus of 2.0 MPa. The Young's modulus of the bulk PDMS was measured using the uniaxial compression test according to Wang *et al.*[30] The pillar in Fig. 2(c) does not look perfectly cylindrical due to its 508 nm high conically shaped tip. Thus, the error in the height of the pillar in the cylindrical model is $\pm 254$ nm. This converts into a systematic error of 1.6nN (13% of the total force) for the cell traction force, estimated by using Eq. (1) and a $5.8\,\mu m$ micropillar height. This error can be reduced by increasing the height of micropillars.

To quantify the tracking precision, we adopted the system error approach proposed by van Hoorn *et al.*[11] In the experiment, all pillars were tracked before cells were plated on pillars to establish zero force references. After cells were plated onto the platform, pillar positions in regions without cells [as shown in the selected region "e" of Fig. 5(a)] were measured and compared with their positions before cell plating. Pillars in these regions are not under the influence of cell forces and in principle do not have any deflection before and after cell loading.

If there is a difference measured before and after cell plating in this cell-empty region, it is due to the system fitting error from the imaging and fitting algorithm. Figure 5(e) displays the histogram plot showing the displacement measured in the region "e." The mean value of these displacements is ~30 nm, which is the pillar position tracking resolution of our method measured by a 20× objective lens. The tracking resolution further improves if a high N.A. objective lens is used.

To conclude, we demonstrated a plasmonic micropillar platform that is capable of providing concurrent and high spatial resolution tracking of micropillar positions across a large FOV. Laser implanted gold nanospheres in micropillars provide strong and point-source-like strong scattering signals that allow precision tracking under a low magnification objective lens. A proof-of-concept demonstration has shown that 30 nm spatial resolution micropillar tracking can be accomplished by using a 20× objective lens with a FOV of $448\,\mu m \times 333\,\mu m$.

See supplementary material for the method of fabricating the plasmonic micropillars.

[1]S. Cross, Y. Jin, J. Rao, and J. Gimzewski, "Nanomechanical analysis of cells from cancer patients," Nat. Nanotechnol. **2**(12), 780–783 (2007).

[2]N. Balaban, U. Schwarz, D. Riveline, P. Goichberg, G. Tzur, I. Sabanay, D. Mahalu, S. Safran, A. Bershadsky, L. Addadi, and B. Geiger, "Force and focal adhesion assembly: A close relationship studied using elastic micropatterned substrates," Nat. Cell Biol. **3**(5), 466–472 (2001).

[3]M. Zündel, A. Ehret, and E. Mazza, "Factors influencing the determination of cell traction forces," PLoS One **12**(2), e0172927 (2017).

[4]J. Tan, J. Tien, D. Pirone, D. Gray, K. Bhadriraju, and C. Chen, "Cells lying on a bed of microneedles: An approach to isolate mechanical force," Proc. Nat. Acad. Sci. **100**(4), 1484–1489 (2003).

[5]J. Fu, Y. Wang, M. Yang, R. Desai, X. Yu, Z. Liu, and C. Chen, "Mechanical regulation of cell function with geometrically modulated elastomeric substrates," Nat. Methods **7**(9), 733–736 (2010).

[6]A. Saez, M. Ghibaudo, A. Buguin, P. Silberzan, and B. Ladoux, "Rigidity-driven growth and migration of epithelial cells on microstructured anisotropic substrates," Proc. Nat. Acad. Sci. **104**(20), 8281–8286 (2007).

[7]L. Trichet, J. Le Digabel, R. Hawkins, S. Vedula, M. Gupta, C. Ribrault, P. Hersen, R. Voituriez, and B. Ladoux, "Evidence of a large-scale mechanosensing mechanism for cellular adaptation to substrate stiffness," Proc. Nat. Acad. Sci. **109**(18), 6933–6938 (2012).

[8]S. Vedula, M. Leong, T. Lai, P. Hersen, A. Kabla, C. Lim, and B. Ladoux, "Emerging modes of collective cell migration induced by geometrical constraints," Proc. Nat. Acad. Sci. **109**(32), 12974–12979 (2012).

[9]M. Reffay, M. Parrini, O. Cochet-Escartin, B. Ladoux, A. Buguin, S. Coscoy, F. Amblard, J. Camonis, and P. Silberzan, "Interplay of RhoA and mechanical forces in collective cell migration driven by leader cells," Nat. Cell Biol. **16**(3), 217–223 (2014).

[10]K. Bashour, A. Gondarenko, H. Chen, K. Shen, X. Liu, M. Huse, J. Hone, and L. Kam, "CD28 and CD3 have complementary roles in T-cell traction forces," Proc. Nat. Acad. Sci. **111**(6), 2241–2246 (2014).

[11]H. van Hoorn, R. Harkes, E. Spiesz, C. Storm, D. van Noort, B. Ladoux, and T. Schmidt, "The nanoscale architecture of force-bearing focal adhesions," Nano Lett. **14**(8), 4257–4262 (2014).

[12]K. Addae-Mensah, N. Kassebaum, M. Bowers, R. Reiserer, S. Rosenthal, P. Moore, and J. Wikswo, "A flexible, quantum dot-labeled cantilever post array for studying cellular microforces," Sens. Actuators A: Phys. **136**(1), 385–397 (2007).

[13]B. Ricart, M. Yang, C. Hunter, C. Chen, and D. Hammer, "Measuring traction forces of motile dendritic cells on micropost arrays," Biophys. J. **101**(11), 2620–2628 (2011).

[14]C. Nelson, S. Raghavan, J. Tan, and C. Chen, "Degradation of micropatterned surfaces by cell-dependent and -independent processes†," Langmuir **19**(5), 1493–1499 (2003).

[15]S. Link and M. El-Sayed, "Spectral properties and relaxation dynamics of surface plasmon electronic oscillations in gold and silver nanodots and nanorods," J. Phys. Chem. B **103**(40), 8410–8426 (1999).

[16]S. Wang, K. Chen, T. Wu, H. Wang, W. Lin, M. Ohashi, P. Chiou, and H. Tseng, "Photothermal effects of supramolecularly assembled gold nanoparticles for the targeted treatment of cancer cells," Angew. Chem. Int. Ed. **49**(22), 3777–3781 (2010).

[17]J. West and N. Halas, "Applications of nanotechnology to biotechnology," Curr. Opin. Biotechnol. **11**(2), 215–217 (2000).

[18]V. Zharov, R. Letfullin, and E. Galitovskaya, "Microbubbles-overlapping mode for laser killing of cancer cells with absorbing nanoparticle clusters," J. Phys. D: Appl. Phys. **38**(15), 2571–2581 (2005).

[19]S. Lee and L. Lee, "Biomolecular plasmonics for quantitative biology and nanomedicine," Curr. Opin. Biotechnol. **21**(4), 489–497 (2010).

[20]T. Wu, T. Teslaa, S. Kalim, C. French, S. Moghadam, R. Wall, J. Miller, O. Witte, M. Teitell, and P. Chiou, "Photothermal nanoblade for large cargo delivery into mammalian cells," Anal. Chem. **83**(4), 1321–1327 (2011).

[21]G. Si, Y. Zhao, J. Lv, M. Lu, F. Wang, H. Liu, N. Xiang, T. Huang, A. Danner, J. Teng, and Y. Liu, "Reflective plasmonic color filters based on lithographically patterned silver nanorod arrays," Nanoscale **5**(14), 6243 (2013).

[22]B. Kiraly, S. Yang, and T. Huang, "Multifunctional porous silicon nanopillar arrays: Antireflection, superhydrophobicity, photoluminescence, and surface-enhanced Raman scattering," Nanotechnology **24**(24), 245704 (2013).

[23]O. du Roure, C. Dequidt, A. Richert, R. H. Austin, A. Buguin, P. Chavrier, P. Silberzan, and B. Ladoux, "Microfabricated arrays of elastomeric posts to study cellular mechanics," Proc. SPIE **5345** (2003).

[24]A. Saez, E. Anon, M. Ghibaudo, O. du Roure, J. Di Meglio, P. Hersen, P. Silberzan, A. Buguin, and B. Ladoux, "Traction forces exerted by epithelial cell sheets," J. Phys.: Condens. Matter **22**(19), 194119 (2010).

[25]S. Ghassemi, G. Meacci, S. Liu, A. Gondarenko, A. Mathur, P. Roca-Cusachs, M. Sheetz, and J. Hone, "Cells test substrate rigidity by local contractions on submicrometer pillars," Proc. Nat. Acad. Sci. **109**(14), 5328–5333 (2012).

[26]H. van Hoorn, E. Spiesz, C. Storm, D. van Noort, B. Ladoux, and T. Schmidt, "High-resolution fluorescence measurements correlated to cellular traction forces," Biophys. J. **104**(2), 193a (2013).

[27]M. Yang, N. Sniadecki, and C. Chen, "Geometric considerations of micro- to nanoscale elastomeric post arrays to study cellular traction forces," Adv. Mater. **19**(20), 3119–3123 (2007).

[28]O. du Roure, A. Saez, A. Buguin, R. Austin, P. Chavrier, P. Silberzan, and B. Ladoux, "Force mapping in epithelial cell migration," Proc. Nat. Acad. Sci. **102**(7), 2390–2395 (2005).

[29]J. Crocker and D. Grier, "Methods of digital video microscopy for colloidal studies," J. Colloid Interface Sci. **179**(1), 298–310 (1996).

[30]Z. Wang, A. A. Volinsky, and N. D. Gallant, "Crosslinking effect on polydimethylsiloxane elastic modulus measured by custom-built compression instrument," J. Appl. Polym. Sci. **131**(22), 41050 (2014).